Garin, Intza; Elli, Francesca M.; Linglart, Agnes; Silve, Caroline; De Sanctis, Luisa; Bordogna, Paolo; Pereda, Arrate; Clarke, Joe T. R.; Kannengiesser, Caroline; Coutant, Regis; Tenebaum-Rakover, Yardena; Admoni, Osnat; De Nanclares, Guiomar Perez; Mantovani, Giovanna. Novel microdeletions affecting the GNAS locus in pseudohypoparathyroidism: Characterization of the underlying mechanisms. THE JOURNAL OF CLINICAL ENDOCRINOLOGY AND METABOLISM. 100 (4) pp: E681-E687. DOI: 10.1210/jc.2014-3098

MICRODELETIONS AFFECTING THE GNAS LOCUS IN PSEUDOHYPOPARATHYROIDISM: CHARACTERIZATION OF THE UNDERLYING MECHANISMS

INTRODUCTION

Pseudohypoparathyroidism type Ia (PHP1A, MIM#103580) is a rare genetic disorder, whose hallmark is end-organ resistance to parathyroid hormone (PTH) due to partial deficiency of the alpha subunit of the stimulatory G protein (Gsα), encoded by the complex imprinted GNAS locus (MIM#139320). PHP1A patients are characterized by PTH resistance, defined as raised serum PTH levels in the presence of hypocalcemia and hyperphosphatemia, and show features of obesity, mental retardation and Albright hereditary osteodystrophy (AHO) (1). PHP1A patients may also develop resistance to thyroid-stimulating hormone (TSH), gonadotropins and growth-hormone-releasing hormone (GHRH) (2, 3).

The disease is inherited in an autosomal dominant manner and, generally, is caused by heterozygous maternally-derived inactivating mutations of Gsα coding exons (1, 4). This pattern of inheritance is consistent with Gsα tissue-specific imprinting and its predominant maternal expression has been indeed demonstrated in specific human tissues, comprising proximal renal tubules, pituitary, gonads, and thyroid (5).

In 1990, Patten et al. described the first *GNAS* loss-of-function mutation responsible for PHP1A (4) and, to date, numerous different Gsα-coding mutations have been identified,

with a detection rate of about 70% (1, 6 and personal data). Most defects are private mutations and few recurrent mutations in unrelated patients probably derived from the presence of a common molecular mechanism rather than a founder effect (7). The detection of a mutation is associated with the development of the disease and 50% of occurrence in the offspring, thus the genetic test provides a diagnosis together with the possibility of genetic counseling in relatives.

Nevertheless, the molecular determinants of 30% patients still remains unclear and, in the last years, different papers described GNAS epigenetic defects, similar to those classically found in PHP−Ib patients, in a subset of patients with PHP and variable degrees of AHO, suggesting a molecular overlap between PHP1A and PHP1B (8).

Recently, some cases of PHP1A patients with deletions of 20q, including part or the whole *GNAS* gene, and an inversion at GNAS were reported, demonstrating that chromosomal rearrangements may also cause PHP1A and that investigation for these less common genetic defects is needed (9). Moreover, deletions ablating GNAS DMRs mimic an imprinting defect during the methylation analysis and may lead to a misdiagnosis of PHP1B (10). These defects, undetectable by Sanger sequencing and often also by karyotype investigation, are considered clearly distinct from the small-scale gene mutations, both for the size of the rearranged DNA and the underlying formation mechanisms (11, 12).

In order to ameliorate molecular diagnostic and genetic counseling, the aims of our work were to identify and characterize novel GNAS locus defects, such as micro-deletions or –duplications, associated with PHP1A/PPHP using methylation specific-

multiplex ligation-dependent probe amplification (MS-MLPA) and custom made CGH array and unravel putative molecular mechanisms responsible for these rearrangements.

PATIENTS AND METHODS

A total of 112 patients with PHP1A/PPHP phenotype and no *GNAS* mutations, all born from non-consanguineous parents, were studied. The clinical diagnosis was based upon the presence of at least two of the six AHO manifestations: brachydactyly (shortening of fourth and/or fifth metacarpals), short stature (height below the 3th percentile for chronological age), obesity (BMI >30 kg/m^2 in adults and >97th centile in children), round face, subcutaneous ossifications (either clinically evident or at X-ray), and mental retardation; when these signs were observed in the presence of PTH resistance (i.e. hypocalcemia, hyperphosphatemia and raised serum PTH levels), PHP1A diagnosis was made. All PHP1A patients showed also resistance to TSH, documented by raised serum TSH levels, absence of anti-thyroid antibodies and presence of a normal thyroid scan.
Patients were studied in different labs, using different techniques. A detailed description of methods is provided as supplementary data (point 1, Supp.Table 1). Informed consent was obtained from all patients and relatives included in the study.

RESULTS

Allele dosage and methylation analysis by MS-MLPA or custom aCGH revealed the presence of 7 heterozygous deletions of part or whole GNAS locus, ranging from 106-bp to 2.6-Mb, in a cohort of 112 GNAS point mutation-negative PHP1A/PPHP probands (detection rate 6.25%).

Six of the seven patients (2 females and 4 males) were affected by PHP1A, and one female patient by PPHP (patient #6). When possible, the parental origin of the deletion was identified and the whole family studied. Main clinical features of deleted patients and affected relatives are described in Table 1. A comprehensive description of novel rearrangements is available in the supplementary data section 2 (Figure 1A/B).

Deletions' breakpoints were subjected to bioinformatic analyses to explore underlying mechanisms and to assess the contribution of the genomic architecture. We analyzed the extent of microhomology at breakpoints and investigated for the presence of known sequence motifs, purine-pyrimidine repeats, AT-content and repetitive elements. An overview of all these results can be found in supplementary data point 3 (Supp.Table 2).

DISCUSSION

In about 70% of cases, PHP1A/PPHP are due to haploinsufficiency caused by maternally/paternally-inherited heterozygous inactivating mutations of the *GNAS* gene (1, 6). A subset of patients not carrying mutations in *GNAS* coding exons might have a deletion removing the entire or part of the *GNAS* gene. Constitutional aberrations of the long arm of chromosome 20 are quite rare, and, to our knowledge, only 7 cases with an interstitial chromosome 20q deletion including *GNAS* have been described in the literature so far (9, 10, 13 - 15).

Here, we report 1 PPHP and 6 PHP1A patients with different submicroscopic deletions including part or the whole GNAS locus. Accordingly, we describe novel deletions in 7/112 probands (6.25%), confirming that these events represent a significant cause of

PPHP/PHP1A, and that, although undetectable by standard PCR-based sequencing, they can be clearly identified by aCGH or MS-MLPA.

For a subset of PHP patients, for whom no mutations are identified by *GNAS* coding region sequencing, the presence of a deletion should be considered for a proper genetic counseling. Indeed, some patients studied for the presence of imprinting defects by methylation-quantitative techniques could be misdiagnosed as PHP1B patients, as previously indicated (10) and now confirmed by patients #1 and #5 of the present work. Unfortunately, a deep phenotypic characterization does not allow to clearly identify a priori the causative molecular defect.

Our findings suggest that some clinical features, namely mental retardation, short stature, round face, brachydactyly, subcutaneous ossifications, are common to most patients, as expected by the removal of *GNAS* Gsα-coding exons. As for the PHP1A phenotype in particular, in accordance with previously reported series showing no genotype/phenotype correlation in this disease (7, 16), in this cohort there is no apparent clinical difference between patients with point mutations and those with GNAS deletions. Moreover, as described for point mutations, intrafamilial differences in phenotypic expression can also be found in those with *GNAS* rearrangements and be not only associated to the imprinting effect (family #2 and #7 of the present report, 13).

Hyperinsulinemia, namely reduced insulin sensitivity, and type 2 diabetes have been recently identified as an additional feature of adult PHP1A (17). On the contrary, complex phenotypes (attention deficit disorder, Evans syndrome, cirrhosis, psoriasis, asthma and bilateral adrenal hyperplasia) may result from a contiguous gene deletion syndrome, as they are hardly explained by *GNAS* haploinsufficiency alone. We

compared our cases with those previously described by 2 other groups and determined the smallest region of overlap (SRO) among deletions, in order to unveil genes contributing to common and, symmetrically, patient-specific clinical features (9, 15~~28~~) (Supp.Figure 1). Patients with a paternal deletion suffered from pre- and post- natal severe growth retardation, dysmorphism, hypotonia and feeding difficulties, but no further similarities can be deduced as 2 cases, with no typical AHO phenotype, were too young and could have developed other signs over the time. As for maternal deletions, there aren't significant differences in involved genes that might explain the reported clinical differences. However, the number of patients with large deletions is too small to speculate the contribution of specific adjacent genes in determining complex phenotypes.

Single or multi-exon rearrangements in GNAS can be routinely screened by MS-MLPA or aCGH (10, 18). However, these diagnostic techniques do not provide detailed information on breakpoints location, so different deletions involving the same exon(s) cannot be distinguished, nor can insight be acquired into the developmental mechanism of these rearrangements. Therefore, we have molecularly characterized the precise deletion boundaries in 5 of the 7 probands and hypothesized the developmental mechanism of these rearrangements.

Genomic deletions can occur during the repair of DNA double strand breaks (DSB's) by several mechanisms: (i) non-replicative repair mechanisms~~:~~—non-homologous end-joining (NHEJ) or non-allelic homologous recombination (NAHR) and (ii) replicative-based repair mechanisms (19).

The major DNA-repair mechanism in humans is NHEJ, either classical with short terminal microhomologies of no more than 4 bp, or non-classical (microhomology-mediated end-joining - MMEJ). The insertion of additional bases at the breakpoint

junction, as in patient #7, is a phenomenon associated to classical NHEJ, which is thus one potential mechanism for this deletion (19).

NAHR, the most common mechanism underlying disease-associated genomic rearrangements and recurrent deletions, occurs between nonallelic homologous sequences, generally repetitive elements of at least 200-bp, such as long or short interspersed nuclear elements (LINE's or SINE's, including Alu-elements) or low copy repeats (LCR's). Diverse studies demonstrated that an high content of Alu-elements results in increased frequency of gene disruption by large deletions in several human diseases, also called Alu-recombination mediated deletion (ARMD)-events (20). We analyzed the regions deleted in our patients for the presence of any of these elements and we found repetitive elements of the same family at both breakpoints in 4 cases (patient #1, #2, #6 and #7), which could indicate NAHR as causative mechanism. Therefore, an Alu-mediated NAHR might result in deletions of patients #2, #6 and #7, while patient #1 showed LINE2 elements at proximal and distal breakpoint junctions.

Alternative mechanisms (NHEJ) appear to be involved in patient #4 deletion, as no repetitive elements were found in the proximity of the breakpoints. The most plausible cause for the deletion of patient #1 is a replicative-based repair mechanism, even though the presence of 2-bp microhomology at the breakpoint junction and deletion-associated DNA sequence motif at the proximal region could also be consistent with classical NHEJ.

Overall, although each deletion event appears to be unique, Alu sequences play a major role in determining the instability of the region. Regardless of the specific recombination mechanism, genomic architectural features have been associated with many rearrangement breakpoints. This suggests that chromosomal rearrangements are

not random events, but result from a predisposition due to the existence of a complex underlying genomic architecture that may create instability in the genome.

In conclusion, our data confirm that *GNAS* deletions must be considered as a possible and significant cause of PPHP/PHP1A. In order to avoid misdiagnosis with PHP1B and to determine the recurrence risk in the offspring, patients negative for point mutations should be further investigated for such rare genetic defects.

ACKNOWLEDGEMENTS

Authors thank physicians, patients and families who permitted to collect and study the series.

REFERENCES

1. Mantovani G. Clinical review: Pseudohypoparathyroidism: diagnosis and treatment. J Clin Endocrinol Metab 2011; 96:3020-3030.

2. Levine MA, Downs RW, Jr., Moses AM, Breslau NA, Marx SJ, Lasker RD, Rizzoli RE, Aurbach GD, Spiegel AM. Resistance to multiple hormones in patients with pseudohypoparathyroidism. Association with deficient activity of guanine nucleotide regulatory protein. Am J Med 1983; 74:545-556.

3. Wemeau JL, Balavoine AS, Ladsous M, Velayoudom-Cephise FL, Vlaeminck-Guillem V. Multihormonal resistance to parathyroid hormone, thyroid stimulating hormone, and other hormonal and neurosensory stimuli in patients with pseudohypoparathyroidism. J Pediatr Endocrinol Metab 2006; 19 Suppl 2:653-661.

4. Patten JL, Johns DR, Valle D, Eil C, Gruppuso PA, Steele G, Smallwood PM, Levine MA. Mutation in the gene encoding the stimulatory G protein of adenylate cyclase in Albright's hereditary osteodystrophy. N Engl J Med 1990; 322:1412-1419.

5. Weinstein LS, Yu S, Ecelbarger CA. Variable imprinting of the heterotrimeric G protein G(s) alpha-subunit within different segments of the nephron. Am J Physiol Renal Physiol 2000; 278:F507-F514.

6. Linglart A, Carel JC, Garabedian M, Le T, Mallet E, Kottler ML. GNAS1 lesions in pseudohypoparathyroidism Ia and Ic: genotype phenotype relationship

and evidence of the maternal transmission of the hormonal resistance. J Clin Endocrinol Metab 2002; 87:189-197.

7. Elli FM, deSanctis L, Ceoloni B, Barbieri AM, Bordogna P, Beck-Peccoz P, Spada A, Mantovani G. Pseudohypoparathyroidism type Ia and pseudo-pseudohypoparathyroidism: the growing spectrum of GNAS inactivating mutations. Hum Mutat 2013; 34:411-416.

8. Perez de Nanclares G, Fernandez-Rebollo E, Santin I, Garcia-Cuartero B, Gaztambide S, Menendez E, Morales MJ, Pombo M, Bilbao JR, Barros F, Zazo N, Ahrens W, Juppner H, Hiort O, Castano L, Bastepe M. Epigenetic defects of GNAS in patients with pseudohypoparathyroidism and mild features of Albright's hereditary osteodystrophy. J Clin Endocrinol Metab 2007; 92:2370-2373.

9. Genevieve D, Sanlaville D, Faivre L, Kottler ML, Jambou M, Gosset P, Boustani-Samara D, Pinto G, Ozilou C, Abeguile G, Munnich A, Romana S, Raoul O, Cormier-Daire V, Vekemans M. Paternal deletion of the GNAS imprinted locus (including Gnasxl) in two girls presenting with severe pre- and post-natal growth retardation and intractable feeding difficulties. Eur J Hum Genet 2005; 13:1033-1039.

10. Fernandez-Rebollo E, Garcia-Cuartero B, Garin I, Largo C, Martinez F, Garcia-Lacalle C, Castano L, Bastepe M, Perez de Nanclares G. Intragenic GNAS Deletion Involving Exon A/B in Pseudohypoparathyroidism Type 1A Resulting in an Apparent Loss of Exon A/B Methylation: Potential for Misdiagnosis of Pseudohypoparathyroidism Type 1B. J Clin Endocrinol Metab 2010; 95:765-771.

11. Gu W, Zhang F, Lupski JR. Mechanisms for human genomic rearrangements. Pathogenetics 2008; 1:4-

12. Lee JA, Carvalho CM, Lupski JR. A DNA replication mechanism for generating nonrecurrent rearrangements associated with genomic disorders. Cell 2007; 131:1235-1247.

13. Mitsui T, Nagasaki K, Takagi M, Narumi S, Ishii T, Hasegawa T. A family of pseudohypoparathyroidism type Ia with an 850-kb submicroscopic deletion encompassing the whole GNAS locus. Am J Med Genet A 2011;

14. Shabtai F, Ben-Sasson E, Arieli S, Grinblat J. Chromosome 20 long arm deletion in an elderly malformed man. J Med Genet 1993; 30:171-173.

15. Aldred MA, Aftimos S, Hall C, Waters KS, Thakker RV, Trembath RC, Brueton L. Constitutional deletion of chromosome 20q in two patients affected with albright hereditary osteodystrophy. Am J Med Genet 2002; 113:167-172.

16. Fernandez-Rebollo E, Lecumberri B, Gaztambide S, Martinez-Indart L, Perez de NG, Castano L. Endocrine profile and phenotype-(epi)genotype correlation in Spanish patients with pseudohypoparathyroidism. J Clin Endocrinol Metab 2013; 98:E996-1006.

17. Muniyappa R1, Warren MA, Zhao X, Aney SC, Courville AB, Chen KY, Brychta RJ, Germain-Lee EL, Weinstein LS, Skarulis MC. Reduced insulin sensitivity in adults with pseudohypoparathyroidism type 1a. J Clin Endocrinol Metab 2013; 98(11):E1796-801.

18. Mantovani G, Linglart A, Garin I, Silve C, Elli FM, de Nanclares GP. Clinical utility gene card for: pseudohypoparathyroidism. Eur J Hum Genet 2013; 21:

19. Shaw CJ, Lupski JR. Implications of human genome architecture for rearrangement-based disorders: the genomic basis of disease. Hum Mol Genet 2004; 13 Spec No 1:R57-R64.

20. Sen SK, Han K, Wang J, Lee J, Wang H, Callinan PA, Dyer M, Cordaux R, Liang P, Batzer MA. Human genomic deletions mediated by recombination between Alu elements. Am J Hum Genet 2006; 79:41-53.

Fig 1A

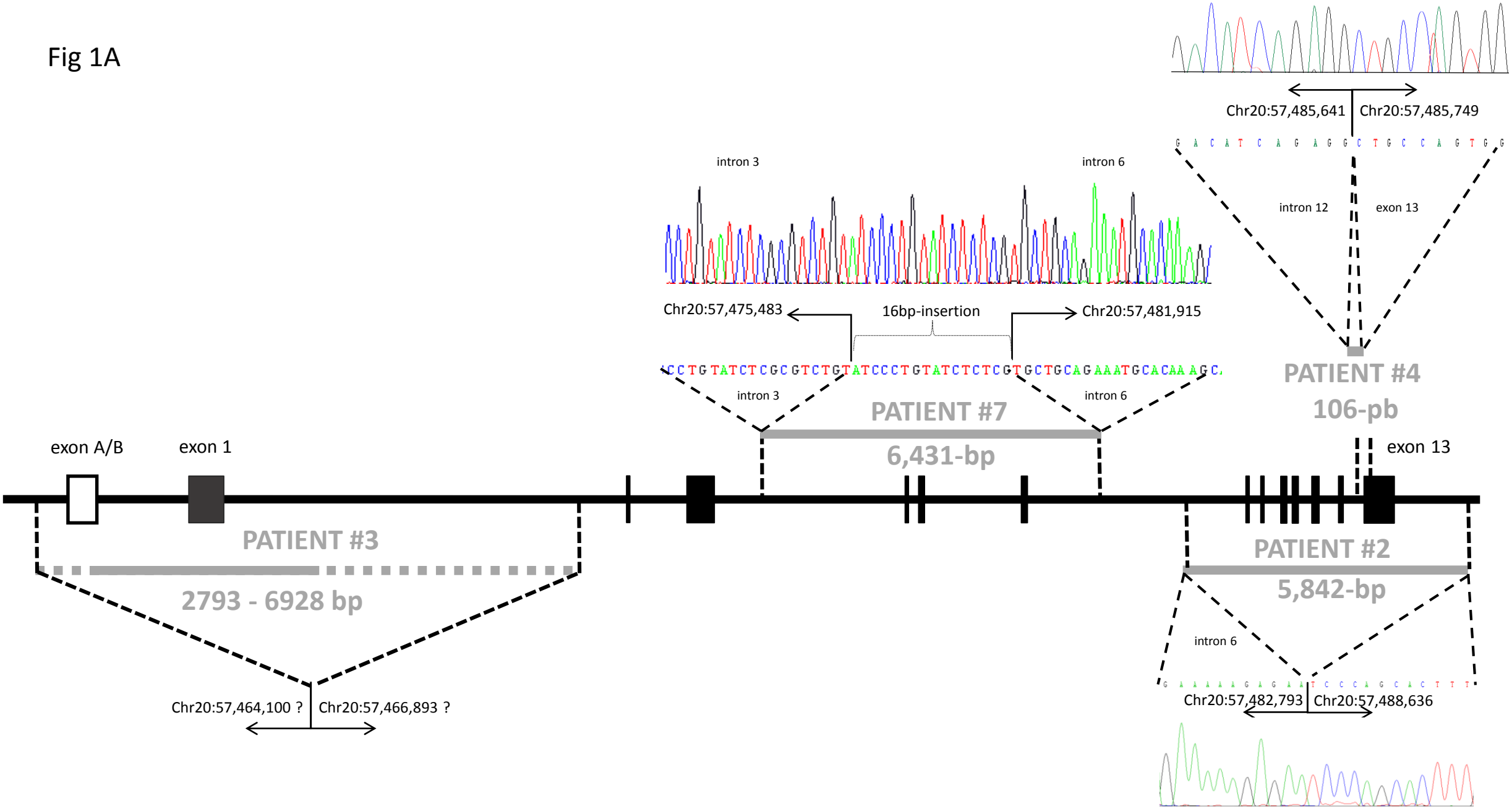
Chr20:57,485,641
Chr20:57,485,749
intron 12
exon 13
PATIENT #4
106-pb
intron 3
intron 6
Chr20:57,475,483
16bp-insertion
Chr20:57,481,915
intron 3
intron 6
PATIENT #7
6,431-bp
exon A/B
exon 1
exon 13
PATIENT #3
2793 - 6928 bp
PATIENT #2
5,842-bp
intron 6
Chr20:57,464,100 ?
Chr20:57,466,893 ?
Chr20:57,482,793
Chr20:57,488,636

Fig 1B

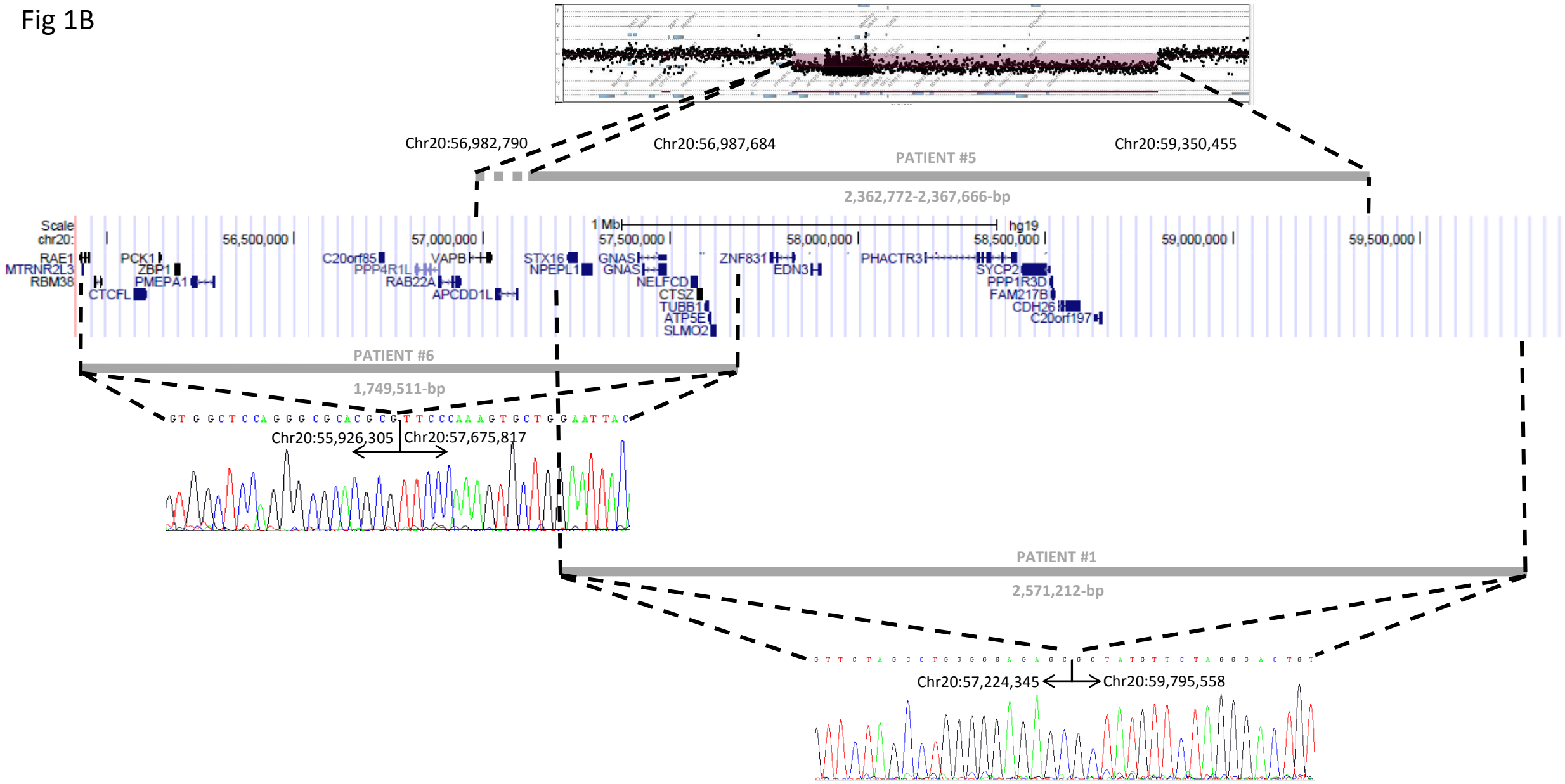
Chr20:56,982,790
Chr20:56,987,684
Chr20:59,350,455
PATIENT #5
2,362,772-2,367,666-bp
Scale
chr20:
1 Mb
hg19
56,500,000
57,000,000
57,500,000
58,000,000
58,500,000
59,000,000
59,500,000
RAE1
MTRNR2L3
RBM38
PCK1
ZBP1
PMEPA1
CTCFL
C20orf85
PPP4R1L
RAB22A
APCDD1L
VAPB
STX16
NPEPL1
GNAS
GNAS
NELFCD
CTSZ
TUBB1
ATP5E
SLMO2
ZNF831
EDN3
PHACTR3
SYCP2
PPP1R3D
FAM217B
CDH26
C20orf197
PATIENT #6
1,749,511-bp
Chr20:55,926,305
Chr20:57,675,817
PATIENT #1
2,571,212-bp
Chr20:57,224,345
Chr20:59,795,558

Table 1: Clinical characteristics and molecular analysis of patients included in the present study

Pt	Sex	Age 1	Age 2	PTH pg/ml	TSH mUI/L	Obesity	AHO features	Additional features	Deletion extension	Deleted Genes
1	M	8	4	206	4.36	Yes	Br/RF/SO/MR	Hyperinsulinemia	g. 57,224,346_59,795,557del	*STX16, NPEPL1, GNAS-AS1, GNAS, NELFCD, CTSZ, TUBB1, SLMO2, ATP5E, ZNF831, EDN3, PHACTR3, SYCP2, PPP1R3D, CDH26*
2a	F	10	0.5	600	14	Yes	Br/RF/MR	-	g.57,482,794_57,488,635del	exon 7_exon 13 of *GNAS*
2b	F	8	0.2	88.3	12.44	No	Br/SO	-	g.57,482,794_57,488,635del	exon 7_exon 13 of *GNAS*
3	M	15	16	342	17.7	No	Br/SS/RF/MR	-	g.(57,463,738_57,464,100)_(57,466,893_57,470,666)del	exon AB_exon 1 of *GNAS*
4	M	40	0.6	312	↑	No	Br/SS/RF/SO	Ankylosing spondilitis	g.57,485,647_57,485,751del	intron 12_exon 13 of *GNAS*
5	M	19	2	478	↑	Yes	SS/SO/MR	Attention deficit disorder, type 2 diabetes, Evans syndrome, cirrhosis, psoriasis, asthma	g.?-56,987,684_59,350,455del	*VAPB, APCDD1L, APCDD1L-AS1, STX16, NPEPL1, GNAS-AS1, GNAS, NELFCD, CTSZ, TUBB1, SLMO2, ATP5E, ZNF831, EDN3, PHACTR3, SYCP2, PPP1R3D, CDH26*
6	F	6	20	21	0.70	Yes	Br/SS	Bilateral adrenal hyperplasia	g.55,926,305_57,675,815del	*MTRNR2L3, RBM38, CTCFL, PCK1, ZBP1, PMEPA1, PPP4R1L, RAB22A, VAPB, APCDD1L, APCDD1L-AS1, STX16, NPEPL1, GNAS-AS1, GNAS, NELFCD, CTSZ, TUBB1, SLMO2, ATP5E* and putatively *RAE1*at the 5'end.
7a	F	1	0.5	277	27	Yes	SS/SO/RF/MR	Craniosynostosis	g.57,475,484_57,481,914del	intron 2_exon 6 of *GNAS*
7b	F	27		120	6	No	SS/SO/MR		g.57,475,484_57,481,914del	intron 2_exon 6 of *GNAS*

Legend: Female (**F**), Male (**M**), Brachydactyly, clinically evident (**Br**), Short Stature (**SS**), Round Face (**RF**), Obesity was defined as BMI >30 kg/m^2 in adults or

weight >97th centile in children, Subcutaneous Ossifications (**SO**), Mental Retardation (**MR**). **Age 1** refers to the age at molecular diagnosis, while **age 2** is the one at clinical diagnosis. PTH and TSH levels refer to the ones at clinical diagnosis, normal values: 10-65 pg/mL for PTH and 0.2-4.0 mUI/L for TSH (unknown levels for patients 4&5 in whom a neonatal diagnosis of primary hypothyroidism was made).

SUPPLEMENTARY INFORMATION

1. DETAILED DESCRIPTION OF MOLECULAR BIOLOGY TECHNIQUES APPLIED TO UNRAVEL AND CHARACTERIZE GNAS STRUCTURAL REARRANGEMENTS IN OUR SERIES

1.1 *GNAS locus MS-MLPA analysis*

Dosage of allele segments and methylation analyses of GNAS locus were carried out by MS-MLPA using the SALSA MLPA ME031 GNAS probemix (MRC-Holland, Amsterdam, The Netherlands) and ABI3130xl and ABI3500 Genetic Analyzers (Perkin-Elmer Corp.), as previously described (S1, S2). Data analysis was performed using GeneMapper software (Applied Biosystems, Foster City, CA) and Coffalyser v9.4 (MRC-Holland, Amsterdam, The Netherlands). A probe ratio below 0.7 for different consecutive probes was considered suggestive of a heterozygous deletion.

1.2 *Genome-wide SNParray*

An Illumina Human660W-Quad BeadChip was run for patients #1 and #5. This array includes 657,366 markers distributed evenly across the genome, with 14,854 markers located on chromosome 20. Images were analyzed using the Chromosome Viewer tool contained in Genome Studio (Illumina, San Diego, CA, USA).

1.3 *Custom CGHarray*

Two independent custom aCGH have been used:

Patients #6 and #7: A custom CGH array was designed to cover by high density the GNAS locus and 15 additional genes localized on chromosome 1, 3, 6, 7, 9, 12, 16, 17, 19, 20, 22 and X (15K oligo array, Agilent Technologies, CA, USA; design ID33306). The GNAS locus (chr20: g.57414773-g.57486255) was covered by a total of 476 probes, and *STX16* gene (exon 3 and 4) by 19 probes (i.e a density of ~ one 60 mer oligonucleotide CGH probe every 150-bp). 1 000-kb flanking 3' and 5' regions at the boundary of the locus were covered by a density of ~ one probe every 4000-bp. On each slide, samples comprised DNA from one control used as reference DNA (identical on each slide), and from 7 patients affected by one pathology putatively associated with a defect in one of the selected genes; therefore samples from non-affected patients for a specific gene served as controls for that gene. Two to four patients affected with PHP were studied on each slide. Array design was validated by analysing samples with previously identified deletion in each gene. Data were analyzed using Feature Extraction V.91.1 and CGH analysis V3.4.27.

Patients #5 and #6: Whole genome analysis was conducted using a custom chromosome 20 focused 4x44k oligonucleotide human array-CGH (AMADID 49562, Agilent Technologies, Santa Clara, CA), following manufacturer's protocol. Custom array covered chr20: g.57,200,000-g.57,500,000 with one probe each 200-bp, whole chromosome 20 with one probe each 2-kb and a backbone with one probe each 300-kb. Commercial healthy male DNA (Promega Biotech, Madison, WI) was used as hybridization control. Microarray data was extracted and visualized using Feature Extraction software v10.7 and Agilent Genomic Workbench v5.0 (Agilent Technologies). Copy number altered regions were detected using ADM-2 (set as 6)

statistic provided by DNA Analytics, with a minimum number of 5 consecutive probes. Genomic build NCBI37 (Hg19) was used for the experiments.

1.4 *Boundaries' delimitation*

As a first step toward the delimitation of deletions, different methods for semiquantitative amplifications were used.

~~Semiquantitative PCR (sq-PCR)~~

Semiquantitative amplification of specific sequences (about 100-bp length) surrounding the region found deleted by MS-MLPA was performed (primers available upon request). Briefly, serial dilutions of wild-type DNA were amplified by non-saturated PCR (20 cycles) together with patients DNA and, after agarose electrophoresis, were analyzed by densitometric scanning of photographs of gels with ImageJ software.

Alternatively, semiquantitative multiplex PCR of short fluorescent fragments (QMPSF) was employed. Firstly, we designed diverse PCR fragments for each flanking region. In the 5'flanking region the reverse primer was marked with fluorescence, whilst in the 3'flanking region the marked primer was forward. These PCRs were performed vs. a known 2 copies region of the genome (as control region) to get a relative semiquantitative PCR (stopped at exponential phase). After the multiplex reaction, the DNA fragments were separated on an ABI3500 Genetic Analyzer and analyzed using GeneMapper software (Applied Biosystems).

To calculate allele dosage we used the numerical sample-to-control comparison. We calculated numerical normalized ratios (R) using the formula: $R=(\text{peak intensity}_{\text{amplicon } x \text{ sample}}/\text{peak intensity}_{\text{amplicon } x \text{ control}})/(\text{peak intensity}_{\text{amplicon ref sample}}/\text{peak intensity}_{\text{amplicon ref control}})$. An R value close to 0.5 (0.4–0.6) represented a 2-fold reduction. As a result we

found regions that were located inside the deletion (PCR relative ratio~0.5) and other regions that were located outside the deletion (PCR relative ratio~1). The objective was to approach as much as possible to the deletion, for the purpose of obtaining a large PCR of the deleted allele and sequences it to identify the breakpoints. This final PCR was run with the nearest to the deletion forward unlabeled primer of the 5'falnking region (in which two copies were observed) and the nearest to the deletion unlabeled reverse of the 3'flanking region (conditions and primers available upon request).

Then, to locate breakpoints at nucleotide level, long range PCRs with primers flanking deleted sequences and a highly performing proofreading polymerase, LA Taq DNA Polymerase (Takara Bio Inc., Otsu, Japan), were performed (conditions and primers available upon request).

Finally, amplicons from deleted alleles were excised from agarose gel after electrophoretic separation, extracted with the MinElute Gel Extraction kit (Qiagen, Hilden, Germany) and sequenced.

1.5 *Parental origin of deletions*

When possible, deletion's parental origin was determined either by long-PCR crossing the boundaries, by microsatellite markers analysis or deduced by the methylation status obtained by MS-MLPA. Three microsatellites were genotyped by migration of the fluorescent- labelled PCR products on a 3130xl Genetic Analyzer (AppliedBiosystems), a 18AC repeat (g.58,304,592-g.58,304,928) localized at the 5' end of the GNAS locus, a 28AC repeat (g.58,439,667-g.58,440,096) within the GNAS locus, and a 19AC repeat (g.58,529,668-g.58,530,005) localized at the 3' end of the GNAS locus.

1.6 *In silico analysis of breakpoint regions*

Breakpoint regions and junction fragments were subjected to an extensive bioinformatic analysis to assess the involvement of the genomic architecture in the origin of the deletions as previously described (S3).

2. DETAILED DESCRIPTION OF NOVEL GNAS STRUCTURAL REARRANGEMENTS IDENTIFIED IN OUR SERIES

2.1 *Short deletions*

Defects detected in patients #2, #3, #4 and #7 were short *GNAS* deletions, affecting only one to seven Gsα-coding exons. The methylation analysis confirmed the absence of imprinting defects for patients #2, #4 and #7.

MS-MLPA investigation of sisters #2a and #2b led to the hypothesis of a deletion encompassing, at least GNAS exons from 7 to 13. Breakpoint characterization and parent's analysis confirmed a maternally-inherited interstitial deletion of 5,842-bp at genomic location g.57,482,794_57,488,635, according to the Genome Reference Consortium Human Build 37 (GRCh37) (Figure 1A). Their mother (#2m) presented only short stature with normal serum calcium, phosphorous and PTH levels.

In patient #4, MS-MLPA revealed a heterozygous deletion within GNAS exon 13 and subsequent analysis showed a 106-bp *de novo* interstitial deletion including part of intron 12 and of exon 13 (genomic location g.57,485,642_57,485,748) (Figure 1A).

According to custom made CGH analysis, patient #7a presented a heterozygous deletion of about 6200-bp extending from intron 2 (first 5'deleted probe at 57,475,366) to intron 5 (last 3'deleted probe at 57,481,550), and thus leading to the partial deletion of introns 2 and 5, and the entire sequence of exons 3, 4 and 5, and introns 3 and 4. MS-MLPA analysis confirmed the deletion. Fine delimitation allowed the identification of a 6,431-bp deletion ranging from locations g.57,475,484 to g.57,481,914. Within the deletion a 16-bp insertion of unknown genetic origin was identified (Figure 1A). The same genetic defect was present in the mother of the patient (#7b).

In patient #3 we observed a deletion encompassing exon A/B to exon 1 revealing a methylation defect limited to the A/B DMR, an imprinting error classically associated with the autosomal dominant inherited form of PHP1B. This deletion could not be delimited at the nucleotide level due to lack of further material, but available data allowed to determine a deletion extension range between 2,793 and 6,928-bp [g.(57,463,738_57,464,100)_(57,466,893_57,470,666)del] (Figure 1A). Parents were not available.

2.2 *Long deletions*

Deletions found in patients #1, #5 and #6 comprised the entire GNAS locus. Methylation analysis of patients #1 and #5 displayed a pattern of loss of imprinting

(LoI) similar to that detected in sporadic PHP1B cases (loss of methylation at AS, XL and A/B DMRs and gain of methylation at NESP DMR), indicating that the maternal allele was ablated. On the contrary, patient #6 presented the opposite methylation pattern, as the deleted allele was the paternal one.

In patient #1, SNP array followed by quantitative PCR and long-PCR revealed the presence of an heterozygous maternally inherited deletion of 2.6-Mb, extending from g.57,224,346 to g.59,795,557 (Figure 1B). The deletion encompassed *STX16, NPEPL1, GNAS-AS1, GNAS, NELFCD, CTSZ, TUBB1, SLMO2, ATP5E, ZNF831, EDN3, PHACTR3, SYCP2, PPP1R3D* and *CDH26* genes. The mother was clinically asymptomatic.

A similar approach was performed for patient #5. The statistical deletion obtained after SNP-array and aCGH extended from g.56,987,684 to g.59,350,455 (size 2,362,772-bp), though data was also compatible with a deletion beginning at 56,982,790 bp (size 2,367,666-bp). Exact breakpoints however could not be determined as it couldn't be amplified and sequenced (Figure 1B). Putatively involved genes are *VAPB, APCDD1L, APCDD1L-AS1, STX16, NPEPL1, GNAS-AS1, GNAS, NELFCD, CTSZ, TUBB1, SLMO2, ATP5E, ZNF831, EDN3, PHACTR3, SYCP2, PPP1R3D* and *CDH26*. The deletion was present in the unaffected mother and the maternal grandfather.

In patient #6 custom made CGH analysis led to the identification of a 1.7-Mb *de novo* deletion extending from g.55,926,306 to g.57,675,816 (Figure 1B). Microsatellite markers genotyping of the proband and her parents confirmed the paternal origin of the deletion. The deletion encompassed *MTRNR2L3, RBM38, CTCFL, PCK1, ZBP1,*

PMEPA1, *PPP4R1L*, *RAB22A*, *VAPB*, *APCDD1L*, *APCDD1L-AS1*, *STX16*, *NPEPL1*, *GNAS-AS1*, *GNAS*, *NELFCD*, *CTSZ*, *TUBB1*, *SLMO2* and *ATP5E* genes, and putatively the 3'-end of *RAE1*.

3. *In silico analysis of breakpoint regions*

In total, 2 of 8 sequence motifs were present. An immunoglobulin heavy chain class switch repeat in the proximal region of patient #1 and deletion hotspot consensus sequence, at the distal region of patient #4. The other breakpoint regions did not contain any known sequence motif.

The analysis of the AT-percentages at sequences located 125-bp down- and upstream of proximal and distal breakpoints showed AT-enriched regions (≥75%) on both breakpoints for patient #2.

The Repeat Masker track in the UCSC genome browser was used to analyze the presence of known repetitive elements intersecting breakpoints. A repetitive element was found at 4 of 5 breakpoints (80%), all of them belonging to the same class, consisting of three Alu- Alu and one LINE2-LINE2 combinations. In these cases, a Blast2 analysis was performed to determine the percentage of sequence identity between the repetitive elements. The highest percentage of sequence identity was observed between Alu elements in patient #2 (88%), while the lowest between LINE2 elements in patient #1 with only 13-bp complementarity in both LINEs.

SUPPLEMENTARY REFERENCES

S1. Elli FM, de SL, Bollati V, Tarantini L, Filopanti M, Barbieri AM, Peverelli E, Beck-Peccoz P, Spada A, Mantovani G. Quantitative analysis of methylation defects

and correlation with clinical characteristics in patients with Pseudohypoparathyroidism type I and GNAS epigenetic alterations. J Clin Endocrinol Metab 2014; 99(3): E508-17.

S2. Fernandez-Rebollo E, Lecumberri B, Garin I, Arroyo J, Bernal-Chico A, Goni F, Orduna R, Castano L, Perez de Nanclares G. New mechanisms involved in paternal 20q disomy associated with pseudohypoparathyroidism. Eur J Endocrinol 2010; 163:953-962.

S3. Jennes I, de JD, Mees K, Hogendoorn PC, Szuhai K, Wuyts W. Breakpoint characterization of large deletions in EXT1 or EXT2 in 10 multiple osteochondromas families. BMC Med Genet 2011; 12:85.

Supplementary Table 1: Brief summary of the techniques employed in the analysis of each patient.

Patient	MS-MLPA	SNP array	Custom aCGH 15k	Custom aCGH 44k	Sq-PCR	QMPSF	Long range PCR
1	✔	✔				✔	✔
2	✔				✔		✔
3	✔						
4	✔				✔		✔
5	✔	✔		✔		✔	
6			✔	✔			✔
7			✔				✔

Supplementary Table 2: Overview of the characteristic of the deletion breakpoints. The positions of the proximal and distal breakpoints or breakpoint regions were given according to the UCSC Human Genome Browser assembly from February 2009 (GRCh37/hg19). Breakpoint sequences are given, including 25 bp down-and upstream from the breakpoints or breakpoint regions if homologous sequences (highlighted in bold) were present at the breakpoint junctions. Down-and upstream borders of the deleted sequences are indicated in small characters. Alternating purine-pyrimidine sequences are underlined. Finally, DNA sequence motifs associated with deletions are marked in grey, while the motif sequence, repetitive elements identified, the identity between the repetitive elements and the plausible molecular mechanisms for each deletion can be found in the last columns. NHEJ (Non-homologous end joining). ARMD (*Alu* recombination-mediated deletion).

Patient	Start (hg19)	End (hg19)	Size (bp)	Breakpoint Sequences	Micro-homology	Repetitive elements (proximal region)	Sequence Motifs (proximal region)	Repetitive elements (distal region)	Sequence Motifs (distal region)	Sequence identity between repetitive elements	Putative molecular mechanism
1	57224346	59795557	2571212	Proximal: ATCACGTTCTAGCCTGGGGGAGAGC**gc**caggaaaagtaaacaggtccccc Distal: tctgacaaatatttttttaagcacttGCTATGTTCTAGGGACTGTAACAAG	2 bp (GC)	L2c	TGGGG	L2a	-	13 bp palindromic sequence	Replicative / Classical NHEJ
2a&2b	57482794	57488635	5842	Proximal: AAGGAAACTCAGAGAAAAAGAGAACaacgcagcttaaaacttttaaaatg Distal: attttttttaatctgaatgcctgtaaTCCCAGCACTTTGGGAGGCCGAGGT	-	AluSg4	-	AluY	-	88%	ARMD
4	57485643	57485747	106	Proximal: TTTTGTTTTCATATGACATCAGAGG**ctg**gctgacagccgtccctggtagg Distal: tgtttgtgcccgcagaggatcagca**CTG**CCAGTGGAGATGGGCGTCACTA	3 bp (CTG)	-	-	-	TGGAGA		Replicative / Classical NHEJ
6	55926306	57675816	1749511	Proximal: AGGAAGTGGCTCCAGGGCGCACGCGcgttgtttccgcggtagtcagggca Distal: cctcaggtgatccactcacctcagcTTCCCAAAGTGCTGGAATTACAGGC	-	AluSq2	-	AluSx	-	85%	ARMD
7	57475484	57481914	6431 + 16pb insertion	Proximal: AGCAATCCCTGTATCTCGCGTCTGTcttctgtcttccttcctttgtctgt Distal: tgtaaagatatcttctgtttgttgaTGC TGCAGAAATGCACAAAGCAGTC	-	AluSx	-	AluSg4	-	84%	Classical NHEJ / ARMD

Supplementary figure 1: Schematic representation of reported deleted regions and genes in the long arm of chromosome 20. The common deleted region in patients with a rearrangement affecting the paternal allele includes genes from *RAE1* to *ATP5E*. Deletions affecting the maternal allele are smaller than paternal ones, and encompasses genes from *STX16* to *CDH26*. The smallest region of overlap (SRO) among all described multigenic deletions of 20q ranges from *STX16* to *ATP5E*.